ARTICLE OPEN

Check for updates

Coding principles and mechanisms of serotonergic transmission modes

Yajun Zhang [1], Peng Zhang [1], Mimi Shin[2], Yuanyu Chang[2], Stephen B. G. Abbott [1], B. Jill Venton[2] and J. Julius Zhu [1,3 ✉]

Serotonin-mediated intercellular communication has been implicated in myriad human behaviors and diseases, yet how serotonin communicates and how the communication is regulated remain unclear due to limitations of available monitoring tools. Here, we report a method multiplexing genetically encoded sensor-based imaging and fast-scan cyclic voltammetry, enabling simultaneous recordings of synaptic, perisynaptic, proximate and distal extrasynaptic serotonergic transmission. Employing this method alongside a genetically encoded sensor-based image analysis program (GESIAP), we discovered that heterogeneous firing patterns of serotonergic neurons create various transmission modes in the mouse raphe nucleus and amygdala, encoding information of firing pulse frequency, number, and synchrony using neurotransmitter quantity, releasing synapse count, and synaptic and/or volume transmission. During tonic and low-frequency phasic activities, serotonin is confined within synaptic clefts due to efficient retrieval by perisynaptic transporters, mediating synaptic transmission modes. Conversely, during high-frequency, especially synchronized phasic activities, or when transporter inhibition, serotonin may surpass transporter capacity, and escape synaptic clefts through 1–3 outlet channels, leading to volume transmission modes. Our results elucidate a mechanism of how channeled synaptic enclosures, synaptic properties, and transporters collaborate to define the coding principles of activity pattern-dependent serotonergic transmission modes.

INTRODUCTION

Serotonergic transmission is involved in a wide array of human behaviors and diseases [1–3]. The sheer number of brain functions influenced by serotonin, encompassing cognition, mood, social interaction, sexual behavior, feeding behavior, motor behavior, reward, motivation, sleep-wake cycle, and thermoregulation, is closely tied to the diverse firing patterns exhibited by serotonergic neurons [4–9]. Despite this connection, for a very long time, it has remained uncertain how these heterogeneous firing patterns might influence serotonin release and signaling, subsequently impacting associated behaviors and diseases [3, 10]. Decades of research, primarily reliant on low-spatial-resolution voltammetry (and microdialysis) experiments that typically detect only extracellular signals [11], postulates serotonin as a volume transmitter that influences many neighboring cells, largely irrespective of firing patterns [12, 13]. However, an electrophysiology study, which, despite relying on indirect calculations and simulation assumptions, estimated remarkably restrained serotonergic transmission [14]. Moreover, selective serotonin reuptake inhibitors (**SSRIs**) are commonly prescribed treatments for depression, but their effects on serotonin reuptake and release are poorly understood [15–17]. Voltammetric studies on SSRIs have fostered a tacitly accepted, nevertheless pharmacologically counterintuitive notion that SSRIs enhance serotonin release [18–21]. Thus, there is a critical need for a reliable, high-resolution method that enables thorough investigations into essential questions surrounding serotonin, its signaling, and functions. Such a method is crucial for our understanding of related behaviors and the development of treatments for associated disorders [10, 22].

In this study, we developed a multiplexed genetically encoded sensor-based imaging and fast-scan cyclic voltammetry (**FSCV**) method to achieve the first simultaneous scrutiny of synaptic, perisynaptic, proximate and distal extrasynaptic transmission. Nanoscopic visualization and transmission property analysis with genetically-encoded sensor-based image analysis program (**GESIAP**) revealed the modes and regulation of serotonergic transmission. Our research in the mouse raphe nucleus and amygdala unveiled that different firing patterns in serotonergic neurons lead to various transmission modes. These modes encode the frequency, number, and synchrony of firing pulses with neurotransmitter quantity, releasing synapse count, and the type of transmission—synaptic or volume. During both (continuous) tonic and low-frequency (burst-like) phasic activities, efficient retrieval by perisynaptic transporters confines serotonin within synaptic clefts, resulting in synaptic transmission. However, during high-frequency or synchronized activities, or when transporters are inhibited, excess serotonin surpasses transporter capacity, diffusing into synaptic clefts through one, sometimes two, and occasionally three outlet channels, initiating volume-based transmission modes. Our findings provide insights into how synaptic structures, properties, and transporters collaborate to regulate serotonergic transmission based on specific neuronal activity patterns.

[1]Departments of Pharmacology, University of Virginia School of Medicine, Charlottesville, VA 22903, USA. [2]Departments of Chemistry, University of Virginia, Charlottesville, VA 22904, USA. [3]School of Pharmaceutical Sciences, Wenzhou Medical University, Wenzhou 325035, China. ✉email: jjzhu-cville@outlook.com

RESULTS

Multiplexed GRAB$_{5HT}$-based imaging and FSCV$_{5HT}$ recordings

To simultaneously monitor synaptic, perisynaptic, and proximate and distal extrasynaptic serotonergic transmission, we multiplexed genetically encoded sensor-based functional imaging and FSCV in a mouse dorsal raphe nucleus ex vivo preparation (Fig. 1A). Specifically, we made Sindbis viral expression of serotonin sensors in the raphe nucleus in vivo and ~18 h after the expression, prepared acute brain raphe slices. Then, we used a local stimulating electrode to activate serotonergic fibers, and simultaneously recorded fluorescence responses in sensor expressing neurons with a Hamamatsu ORCA FLASH4.0 camera and voltammetric responses with a Nafion-coated carbon-fiber microelectrode placed next to sensor expressing neurons (Fig. 1B). Using Nafion-coated carbon-fiber microelectrodes with a serotonin-specific Jackson FSCV voltage waveform permitted serotonin-specific fast-scan cyclic voltammetry (FSCV$_{5HT}$) detection (Fig. S1; cf. [23, 24]). To selectively image serotonergic fluorescence responses, we first tested two newly developed genetically encoded serotonin sensors, GRAB$_{5HT}$ [25] and iSeroSnFR [26], in cultured hippocampal slices (Fig. S2A), a preparation routinely employed for rapid sensor testing [25, 27, 28]. While a brief 10-ms puff of serotonin evoked fluorescence responses in both GRAB$_{5HT}$ and iSeroSnFR expressing neurons, more robust $\Delta F/F_0$ responses were recorded in GRAB$_{5HT}$ than iSeroSnFR expressing neurons, particularly when a physiological concentration of serotonin was applied (Fig. S2B, C). Thus, GRAB$_{5HT}$ was chosen for all further experiments. To confirm the specificity of $\Delta F/F_0$ responses detected by GRAB$_{5HT}$, which is engineered based on the serotonin 2C receptor [25], we bath applied RS102221, a selective antagonist of the receptor [29], in an ex vivo preparation of the mouse dorsal raphe nucleus, a brain area known for prominent serotonin signals [3]. Bath application of RS102221 abolished the fluorescence responses evoked by a train of 20 electric pluses delivered at 64 Hz, but not voltammetric responses at GRAB$_{5HT}$ expressing neurons (Fig. S2D–H), verifying the specificity of GRAB$_{5HT}$ fluorescence responses.

Serotonergic neurons display a spectrum of firing patterns intricately linked to various behaviors, yet uncovering the precise impact of these firing activities on serotonin release and signaling remains a persistent challenge. In the mouse dorsal raphe nucleus ex vivo preparation, we applied electric stimulations that simulated low-frequency tonic firing at ~2 Hz, short burst firing at ~8, ~25, ~32, and ~64 Hz (Fig. 1C–E), which are associated with behaviors related to wakefulness or alertness, reward expectations, sensory stimuli or natural rewards, unexpected rewards, and sexual or social rewards, respectively [4–9]. We found that only high frequency, high intensity stimuli induced both GRAB$_{5HT}$ fluorescence and FSCV$_{5HT}$ voltammetric responses (Fig. 1C–E). To examine whether the responses depend on the recruitment of more presynaptic axons as electric stimulation intensity increases, we applied a minimal stimulation protocol. Figure 1C, D showed that low-intensity stimuli (3.0, 3.5, 4.0, and 4.5 V) of 5 pulses at 64 Hz evoked neither GRAB$_{5HT}$ fluorescence nor FSCV$_{5HT}$ voltammetric responses. Higher intensity stimuli (5.0, 6.0, and 7.0 V) elicited small, consistent GRAB$_{5HT}$ fluorescence responses, but no FSCV$_{5HT}$ responses. Even higher intensity stimuli (8.0 and 9.0 V) doubled the size of GRAB$_{5HT}$ fluorescence responses, still without FSCV$_{5HT}$ responses. Only the highest intensity stimuli (10.0 V) elicited both tripled-sized GRAB$_{5HT}$ fluorescence responses and FSCV$_{5HT}$ voltammetric responses. These findings suggest that the activation of single serotonergic axons usually results in constrained serotonergic transmission. However, the synchronized activation of multiple serotonergic axons or neuronal pools, as observed in emotional behaviors [30], leads to serotonin dispersion beyond individual GRAB$_{5HT}$ expressing neurons, as detected by FSCV$_{5HT}$, indicating volume transmission. Additionally, lower frequency stimuli, including 5-pulse stimuli at 8, 25, and 32 Hz, along with 20-pulse stimuli at 2 Hz, consistently elicited GRAB$_{5HT}$ fluorescence responses without observable FSCV$_{5HT}$ voltammetric responses across the entire examined intensity range (Fig. 1E), suggesting a restricted serotonergic transmission.

We conducted further quantitative analysis of GRAB$_{5HT}$ fluorescence responses using a genetically encoded sensor-based image analysis program (**GESIAP**) [31], enabling visualization of serotonin diffusion at individual releasing synapses (Fig. 1F). The analysis revealed that instances of low GRAB$_{5HT}$ fluorescence responses ($<\sim 0.60\%$ $\Delta F/F_0$) or low percentages of individual releasing synapses exhibiting an expanded serotonin diffusion profile ($<\sim 33\%$) were seldom accompanied by FSCV$_{5HT}$ voltammetric responses (Fig. 1G–H). Only heightened activity could result in enhanced serotonin release and expanded serotonin diffusion, and evident volume transmission (Fig. 1G–H).

Transporters control serotonin reuptake but not release

To determine whether serotonin transporters control serotonin dispersion beyond individual GRAB$_{5HT}$ expressing neurons, we examined the impact of escitalopram, a potent selective serotonin transporter inhibitor [18, 32], on simultaneously recorded GRAB$_{5HT}$ fluorescence and FSCV$_{5HT}$ voltammetric responses in the mouse dorsal raphe nucleus ex vivo preparation. Bath application of escitalopram prolonged the time course of both GRAB$_{5HT}$ fluorescence and FSCV$_{5HT}$ voltammetric responses evoked a train of 10-pulse stimuli delivered at 64 Hz, although it enhanced the amplitude of only FSCV$_{5HT}$ voltammetric responses but not GRAB$_{5HT}$ fluorescence responses (Fig. 2A–E). The results suggest that escitalopram enhances extracellular serotonergic transmission, consistent with previous FSCV$_{5HT}$-based voltammetric studies [18–21]. However, our GRAB$_{5HT}$-based imaging suggests an alternative mechanism that is mediated by inhibiting reuptaking the transmitter without increasing its release.

To verify the findings, we directly measured the effect of escitalopram on the release properties of serotonergic transmission using the genetically encoded sensor-based image analysis program (**GESIAP**) [31]. Bath application of escitalopram lengthened the decay time course of evoked fluorescence GRAB$_{5HT}$ responses without altering the rise time, and it did not change the number of releasing synapses at GRAB$_{5HT}$ expressing neurons that were visualized with GESIAP (Fig. 3A–C; Movie S1). Application of trains of electric pulses at 0.1 Hz evoked $\Delta F/F_0$ responses at single releasing synapses of GRAB$_{5HT}$ expressing neurons that appeared as stochastic failures and release events (Fig. 3D). Bath application of tetrodotoxin (**TTX**), which blocks action potential-dependent synaptic transmission [33], resulted in elimination of the quantal release events (Fig. S3), confirming the synaptic origin of the signals (cf. [31, 34]). Moreover, the bath application of TTX revealed the low occurrence of TTX-insensitive quantal events (0 events per 5–10 min, $n = 6$ neurons from 5 animals), suggesting a high dependence of transmitter release on action potentials. These evoked fluorescence responses were fit with a double-exponential synaptic function using MATLAB algorithms in GESIAP, providing estimates of key parameters such as rise time, decay time constant, and amplitude [31, 35]. Escitalopram did not alter the rise time of quantal release events but did enhance the decay time constant of quantal responses (Fig. 3E, F). Plotting $\Delta F/F_0$ amplitude histograms, an analysis method adapted from the classic quantal analysis approach [36], revealed multiple, nearly equally spaced peaks, and analysis yielded the same number of released vesicles (average ~1.3 vesicular quanta and up to 3–4 vesicular quanta per stimulus) before or after bath application of escitalopram (Fig. 3G–I). In addition, the analysis enabled direct readout of the same vesicular quantal size of ~0.45% $\Delta F/F_0$ for serotonin and the same release probability P_r of ~0.80 (release success rate over multiple trials) at single releasing synapses
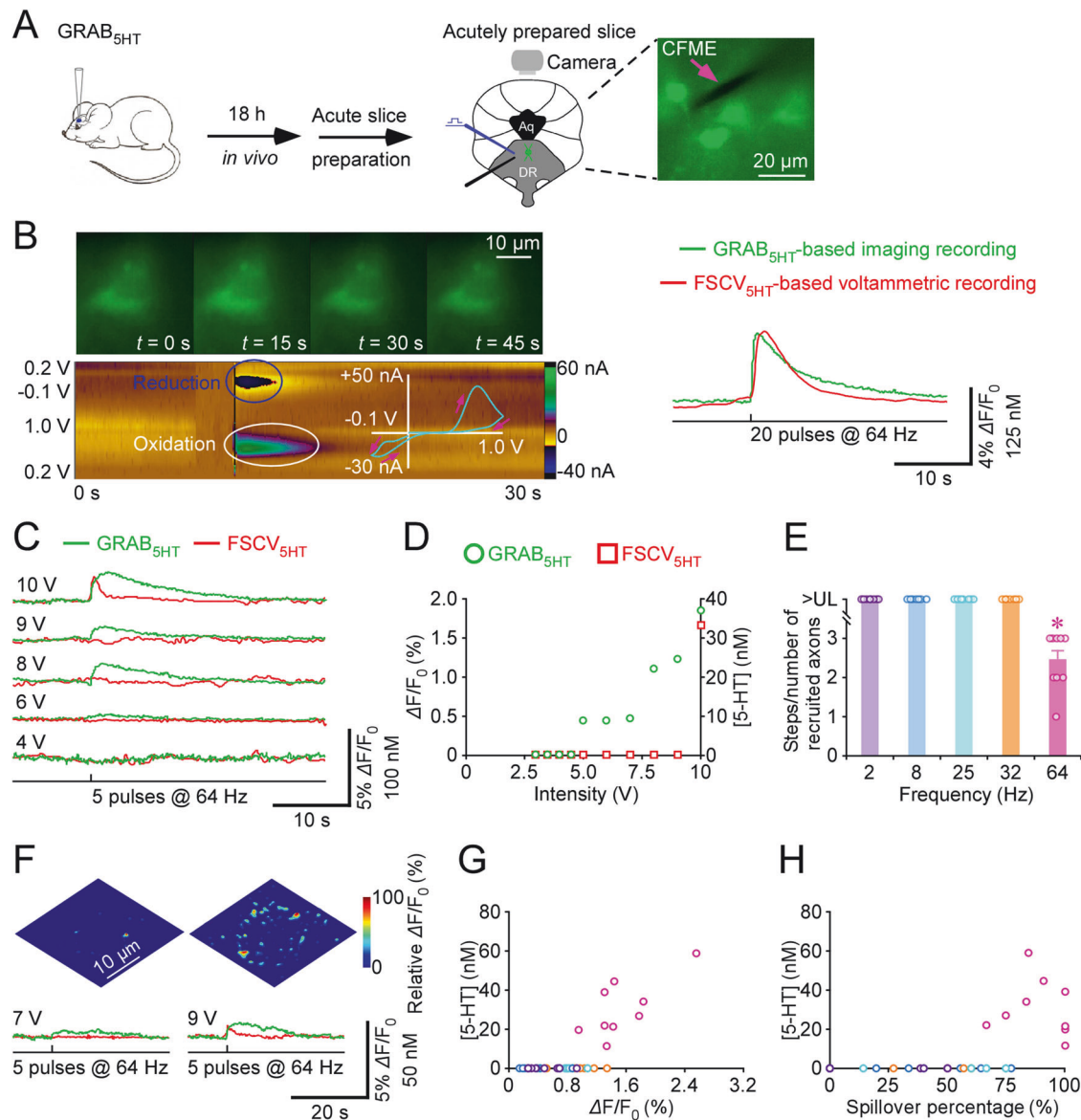
Fig. 1 Simultaneous GRAB₅HT- and FSCV₅HT-based recordings of serotonergic transmission. A Schematic of experimental design illustrating multiplexed imaging and voltammetry conducted in a mouse dorsal raphe nucleus (**DR**) slice preparation. The image on the right depicts the placement of a carbon fiber microelectrode (**CFME**), highlighted by a pink arrow, in proximity to $GRAB_{5HT}$ expressing neurons marked by an orange arrow. Note the distance between CFMEs and imaged expressing neurons in paired recordings, ranging from 12 to 48 μm (26.6 ± 5.8 μm; $n = 9$ pairs from 9 animals). **B** Left, snapshots of fluorescence $\Delta F/F_0$ responses (upper) and a color plot of cyclic voltammogram (lower) of electrically evoked serotonin release at a $GRAB_{5HT}$ expressing raphe neuron. Right, simultaneous $GRAB_{5HT}$-based imaging and $FSCV_{5HT}$-based voltammetric recording traces. **C** $GRAB_{5HT}$ and $FSCV_{5HT}$ recording traces capturing serotonin release in response to stimulus trains composed of 5 pulses at 64 Hz at varied intensities. Note the stepwise increase in $GRAB_{5HT}$ fluorescence $\Delta F/F_0$ responses, suggesting the recruitment of more axons with elevated stimulus intensity. **D** Maximal fluorescence $\Delta F/F_0$ responses and serotonin concentrations measured with $GRAB_{5HT}$ (green) and $FSCV_{5HT}$ (red) in response to the stimulus trains. **E** Summary of $GRAB_{5HT}$ response steps (presumably equivalent to the number of recruited axons) required to trigger $FSCV_{5HT}$ signals under various stimulation parameters (20 pulses at 2 Hz: >upper limit, $n = 9$ neurons from 5 animals; 5 pulses at 8 Hz: >upper limit, $n = 7$ neurons from 4 animals; 5 pulses at 25 Hz: >upper limit, $n = 8$ neurons from 5 animals; 5 pulses at 32 Hz: >upper limit, $n = 7$ neurons from 4 animals; 5 pulses at 64 Hz: 2.44 ± 0.24, $n = 9$ neurons from 5 animals). The step required for 5 pulses at 64 Hz ($p < 0.001$, $U = 0.00$) were significantly smaller than those for 20 pulses at 2 Hz. Asterisks indicate $p < 0.05$ (Rank Sum non-parametric tests). **F** Heatmaps of electrically evoked $GRAB_{5HT}$ fluorescence $\Delta F/F_0$ responses, and $GRAB_{5HT}$ and $FSCV_{5HT}$ recording traces in response to 5 pulses 64 Hz stimuli delivered at voltages of 7 and 9 V. Scale bars applied to all in **F**. **G** Plot of voltammetric $FSCV_{5HT}$ responses against fluorescence $\Delta F/F_0$ responses in response to 20 pulses delivered at 2 Hz, 5 pulses at 8, 25, 32 and 64 Hz. Note the occurrence of voltammetric $FSCV_{5HT}$ responses corresponding to a minimum of 0.60% $GRAB_{5HT}$ fluorescence $\Delta F/F_0$. **H** Plot of voltammetric $FSCV_{5HT}$ responses against percentages of individual releasing synapses showing an expanded serotonin diffusion profile in response to 20 pulses delivered at 2 Hz, 5 pulses at 8, 25, 32, and 64 Hz. Note the occurrence of voltammetric $FSCV_{5HT}$ responses corresponding to a minimum of 32.86% individual release sites exhibiting the expanded serotonin diffusion profile.
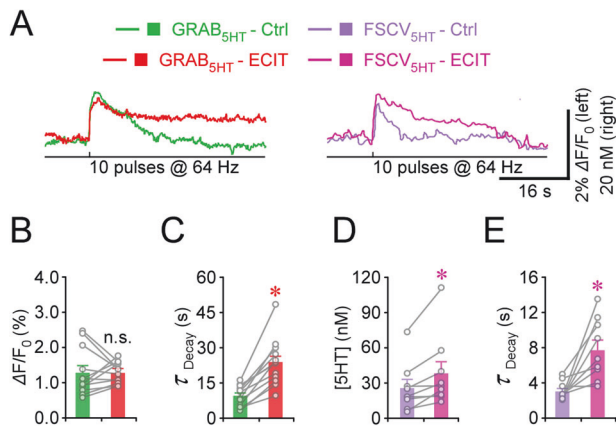
Fig. 2 Serotonin transporter inhibition enhances serotonin signals. A Simultaneous $GRAB_{5HT}$ and $FSCV_{5HT}$ recordings of evoked voltammetry and fluorescence $\Delta F/F_0$ responses before (green and red) and after (purple and pink) the bath application of 10 µm escitalopram (**ECIT**). **B–C** Peak amplitudes (Ctrl: 1.26 ± 0.19%; ECIT: 1.27 ± 0.08%, $Z = 0.24$, $p = 0.85$, $n = 12$ neurons from 6 animals) and decay time constants (Ctrl: 9.74 ± 1.25 s; ECIT: 23.84 ± 2.88 s, $Z = 3.06$, $p < 0.001$, $n = 12$ neurons from 6 animals) of $GRAB_{5HT}$ fluorescence $\Delta F/F_0$ responses before (green) and after (red) the bath application of ECIT. **D–E** Peak amplitudes (Ctrl: 25.67 ± 6.73 nM; ECIT: 38.22 ± 10.00 nM, $Z = 2.66$, $p < 0.001$, $n = 9$ neurons from 6 animals) and decay time constant (Ctrl: 3.09 ± 0.34 s; ECIT: 7.76 ± 1.14 s, $Z = 2.66$, $p = 0.004$, $n = 9$ neurons from 6 animals) of $FSCV_{5HT}$ voltammetric responses before (purple) and after (pink) the bath application of ECIT. Asterisks indicate $p < 0.05$ (Wilcoxon tests).

before and after bath application of escitalopram (Fig. 3J–K). These results confirm that escitalopram prolongs serotonergic signals by inhibiting reuptake without affecting serotonin release.

To independently corroborate our findings in a different brain region, we investigated the effect of escitalopram on serotonin diffusion in an ex vivo amygdalar preparation, another brain area with prominent serotonin signals [3]. When escitalopram was introduced into the bath solution, we observed a prolonged decay time course of evoked fluorescence responses at $GRAB_{5HT}$ expressing amygdalar neurons, while the response amplitude remained unchanged (Fig. 4A–D). We did not observe any significant alterations in the number of releasing synapses at $GRAB_{5HT}$ expressing amygdalar neurons (Fig. 4E, F). Moreover, while escitalopram did not affect the rise time of quantal release events, it notably extended the decay time constant of these responses (Fig. 4G, H). Quantal analysis revealed consistent numbers of released vesicles, averaging ~1.3 vesicular quanta, occasionally up to 2–3 vesicular quanta per stimulus before and after escitalopram application (Fig. 4I, J). Furthermore, this analysis showed the same vesicular quantal size of ~0.45% $\Delta F/F_0$ for serotonin and the release probability at single releasing synapses remained unchanged, maintaining a value of ~0.80 at single releasing synapses before and after escitalopram application (Fig. 4K). Together, these results suggest that the escitalopram-induced inhibition of transporters prolongs serotonergic signals without directly affecting the release of serotonin itself.

To further validate our observations using an alternative pharmacological inhibitor, we employed paroxetine, a more potent serotonin transporter inhibitor [18], in the mouse ex vivo amygdalar preparation. Paroxetine prolonged the decay time course of evoked fluorescence $GRAB_{5HT}$ responses without altering the response magnitude (Fig. S4A–D). Moreover, the quantity of releasing synapses in these neurons remained unchanged (Fig. S4E, F). Once again, paroxetine did not impact the rise time of quantal release events but significantly prolonged their decay time constant (Fig. S4G, H). Quantitative analysis consistently indicated similar numbers of released vesicles,

averaging ~1.2 vesicular quanta and occasionally up to 2–3 vesicular quanta per stimulus before and after paroxetine application (Fig. S4I, J). Additionally, this analysis reaffirmed a consistent vesicular quantal size of ~0.40% $\Delta F/F_0$ for serotonin, maintaining an unaltered release probability of ~0.80 at single releasing synapses before and after paroxetine application (Fig. S4I, J). Collectively, these findings consistently support the notion that transporter inhibition extends serotonergic signals without directly influencing serotonin release.

Somatic and dendritic releasing synapses share the same properties

At times, 1–2 dendrites were observed in the same focal plane as the soma of $GRAB_{5HT}$ expressing neurons in the amygdalar preparation, enabling simultaneous imaging of $GRAB_{5HT}$ fluorescence responses at single releasing synapses on both the soma and dendrites of $GRAB_{5HT}$ expressing neurons (Fig. 5A). The evoked quantal events at these locations exhibited the identical rise times and decay time constants (Fig. 5B–D). Synaptic properties at somatic and dendritic synapses were consistent, with an average of ~1.2 vesicular quanta per stimulus and occasional events of 2–3 vesicular quanta (Fig. 5E). The vesicular quantal size was ~0.40–0.45% $\Delta F/F_0$ for serotonin, with a release probability P_r of ~0.80 at both somatic and dendritic synapses (Fig. 5F, G). These results suggest that the basic properties of serotonergic synapses are conserved between the soma and dendrites, reinforcing the idea that these properties are consistent across various brain areas and animal species [31, 34].

Given the consistent vesicular quantal size across all synapses, we sought to estimate the amount of serotonin released during quantal events, which remains unclear due to limitations in current detection methods, such as electrochemistry, microdialysis, and fluorescent sensor-based photometry [11, 37]. To address this, we calibrated the serotonin concentration-fluorescence response curve for $GRAB_{5HT}$, which was fitted with a sigmoidal function (Fig. S5). Using this function, we converted the vesicular quantal size of ~0.45% $\Delta F/F_0$ to an estimated ~100 nM of serotonin at individual releasing synapses on both the soma and dendrites.

Transporters gate serotonin egress at synapses

To understand how serotonin transporters influence serotonin after its release, we used GESIAP to analyze the spatial diffusion of released serotonin at synaptic, perisynaptic, and extrasynaptic areas, before and after bath application of escitalopram in the dorsal raphe nucleus (Fig. 6A). We typically identified individual releasing synapses with 10-pulse stimuli delivered at 64 Hz first, and then analyzed the spatial diffusion of serotonin released by 10-pulse stimuli delivered at 16 Hz. GESIAP created the serotonin spatial diffusion profiles with pixel-wise maximal $\Delta F/F_0$ plots, revealing that under the normal condition, serotonin diffusion at those well-isolated releasing synapses fit well with a single-exponential decay function that yielded a serotonin spread length constant of ~0.75 µm at raphe neurons (Fig. 6B, C). In the presence of escitalopram, pixel-wise maximal $\Delta F/F_0$ plots floated upwards at ~0.5 µm away from the releasing synapses (Fig. 6B, C). Arbitrarily fitting the plots with a single-exponential decay function gave an estimation of a larger serotonin spread length constant of ~0.85 µm at raphe neurons (Fig. 6C), indicating a significant effect of escitalopram on spatial diffusion of released serotonin.

The high-resolution serotonin spatial diffusion profiles created with GESIAP allowed us to zoom into those well-isolated releasing synapses, revealing that under the normal condition, serotonin concentration rapidly dropped as it diffused away from the release center, forming typically a circle cone-like profile with a full width at half maximum (**FWHM**) of ~0.5 µm, the size about synapses (Fig. 6D, E; Movie S2). Escitalopram enlarged the diffusion profiles and revealed 1–3 egress outlets that channeled serotonin for
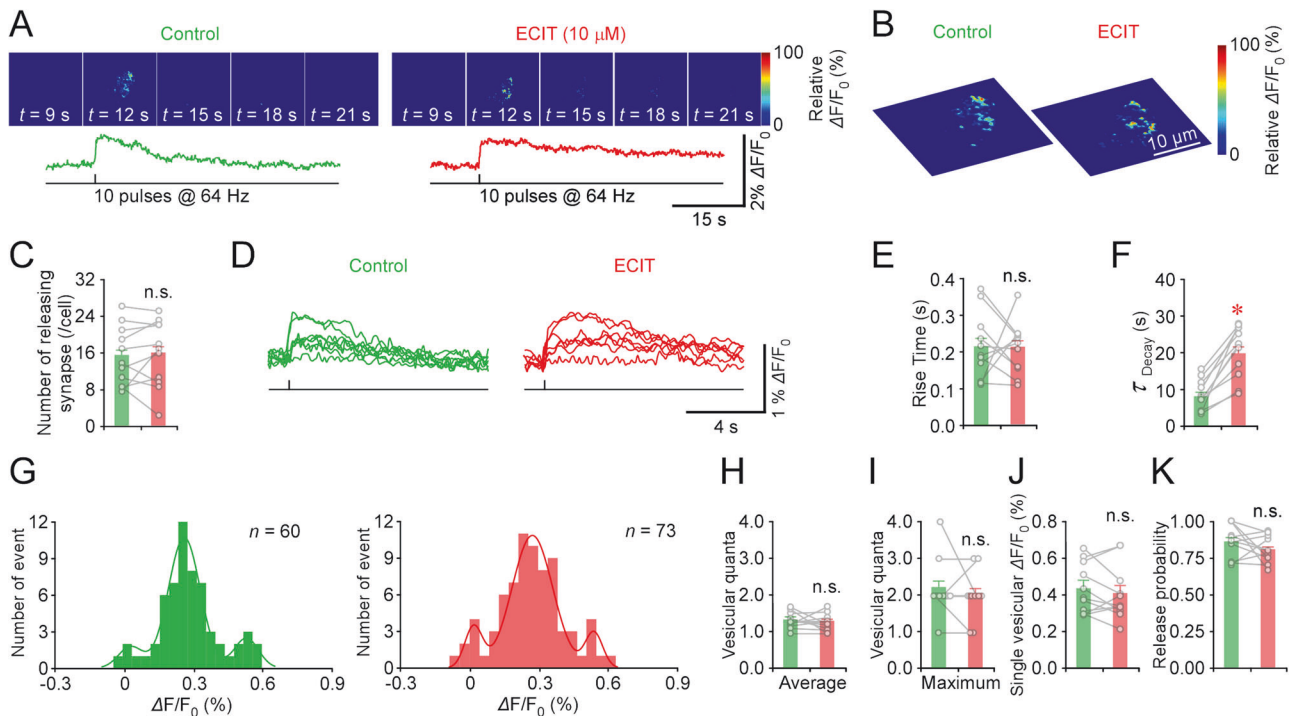
Fig. 3 Transporter inhibition prolongs serotonin signals without altering release properties. A Heatmaps of electrically evoked fluorescence $\Delta F/F_0$ responses before (left) and after (right) the bath application of 10 μm escitalopram (**ECIT**). **B** 3D spatiotemporal profiling of electrically evoked fluorescence $\Delta F/F_0$ responses before (left) and after (right) the bath application of ECIT. Scale bars applied to all in **A**, **B**. **C** Releasing synapse counts before (green) and after (red) the bath application of ECIT (Ctrl: 15.45 ± 1.86; ECIT: 16 ± 2.10; $Z = 0.36$, $p = 0.76$, $n = 11$ neurons from 5 animals). **D** Ten $\Delta F/F_0$ responses evoked by single pulse stimuli at isolated releasing synapses before (green) and after (red) the bath application of ECIT. **E–F** 10–90% rise times (Ctrl: 0.21 ± 0.03 s; ECIT: 0.21 ± 0.02 s; $Z = -0.36$, $p = 0.76$, $n = 11$ neurons from 5 animals) and decay time constants (Ctrl: 8.22 ± 1.18; ECIT: 19.68 ± 2.04; $Z = 2.93$, $p < 0.001$; $n = 11$ neurons from 5 animals) of $\Delta F/F_0$ responses before (green) and after (red) the bath application of ECIT. **G** Amplitude histograms of $\Delta F/F_0$ responses before (green) and after (red) the bath application of ECIT. **H–K** Average (Ctrl: 1.34 ± 0.06; ECIT: 1.28 ± 0.07; $Z = -0.46$, $p = 0.69$, $n = 11$ neurons from 5 animals) and maximal (Ctrl: 2.18 ± 0.22; ECIT: 2 ± 0.19; $Z = -0.46$, $p = 0.69$, $n = 11$ neurons from 5 animals) vesicular quanta, quantal sizes (Ctrl: $0.44 \pm 0.04\%$; ECIT: $0.41 \pm 0.04\%$; $Z = -0.89$, $p = 0.41$, $n = 11$ neurons from 5 animals), and release probabilities (Ctrl: $86.32 \pm 3.4\%$; ECIT: $80.69 \pm 2.72\%$; $Z = -1.33$, $p = 0.21$, $n = 11$ neurons from 5 animals). Asterisks indicate $p < 0.05$ (Wilcoxon tests).

3–5 μm towards the extrasynaptic space, which altered the profile to an ellipse cone-like sharp with a minor axis FWHM of ~0.5 μm and a major axis FWHM of ~1.0 μm, effectively doubling its aspect ratio and halving its roundness value (Fig. 6D–F). As a control, we found that repetitively evoking serotonin release did not change the serotonin diffusion profile and spread length constant at raphe neurons (Fig. S6). Quantitative analysis of the diffusion profiles revealed that escitalopram had little effect on serotonin accumulation and diffusion within the radius of ~0.5 μm from the release center (synaptic sites), enhanced serotonin accumulation and slowed its diffusion between the radii of ~0.5–3 μm from the release center (perisynaptic sites), and slightly increase serotonin buildup at ~3 μm or more from the release center (proximate extrasynaptic sites) (Fig. 6G, H). These results indicate the primary effect site of escitalopram to be ~0.5–3 μm from the release center, the perisynaptic area where serotonin transporters are highly expressed [38–40].

In the amygdalar preparation, we confirmed the impact of transporters on serotonin diffusion. Once more, the effect of escitalopram was evident in broadening the serotonin diffusion at GRAB$_{5HT}$ expressing amygdalar neurons (Fig. S7A–C). This alteration transformed the diffusion profile from a circular cone-like shape to an elliptical cone-like form, revealing 1–3 egress channels through which serotonin traveled ~1–5 μm to reach the extracellular space (Fig. S7D–F). Specifically, escitalopram exhibited minimal effect on serotonin accumulation and diffusion within a radius of ~0.5 μm from the release center, the synaptic sites. However, it notably intensified serotonin accumulation and

slowed its diffusion between radii of ~0.5–3 μm from the release center, the perisynaptic sites. Furthermore, it marginally increased serotonin buildup at distances of ~3 μm or more from the release center, the proximate extrasynaptic sites (Fig. S7G, H). Together, these results elucidate the impact of escitalopram on post-released serotonin diffusion in general.

We further verified the findings with the potent serotonin transporter inhibitor, paroxetine, in the mouse amygdalar preparation. Similar to escitalopram, paroxetine expanded serotonin diffusion at GRAB$_{5HT}$ expressing amygdalar neurons, reshaping the diffusion pattern from a circular cone-like to an elliptical cone-like shape. This transformation revealed 1–3 pathways through which serotonin traveled ~1–5 μm before dispersing into the extracellular space (Fig. S8A–G). Once again, akin to escitalopram, paroxetine had minimal impact on serotonin accumulation and diffusion within a radius of ~0.5 μm from the release center, increased serotonin accumulation and slowed its diffusion between radii of ~0.5–3 μm from the release center, and marginally elevated serotonin buildup at distances of ~3 μm or more from the release center (Fig. S8H, I).

To eliminate the possibility of nonspecific involvement by other neurotransmitters, we conducted two sets of control experiments. First, bath application of inhibitors targeting AMPA receptors (**-Rs**), NMDA-Rs, GABA$_A$-Rs, and GABA$_B$-Rs, using NBQX, AP5, PTX, and CGP, respectively, showed no discernible influence on the serotonin diffusion profile (Fig. S9). Furthermore, we made in vivo AAV viral expression of Cre-dependent ChrimsonR-tdTomato in the dorsal raphe nucleus followed by Sindbis viral expression of
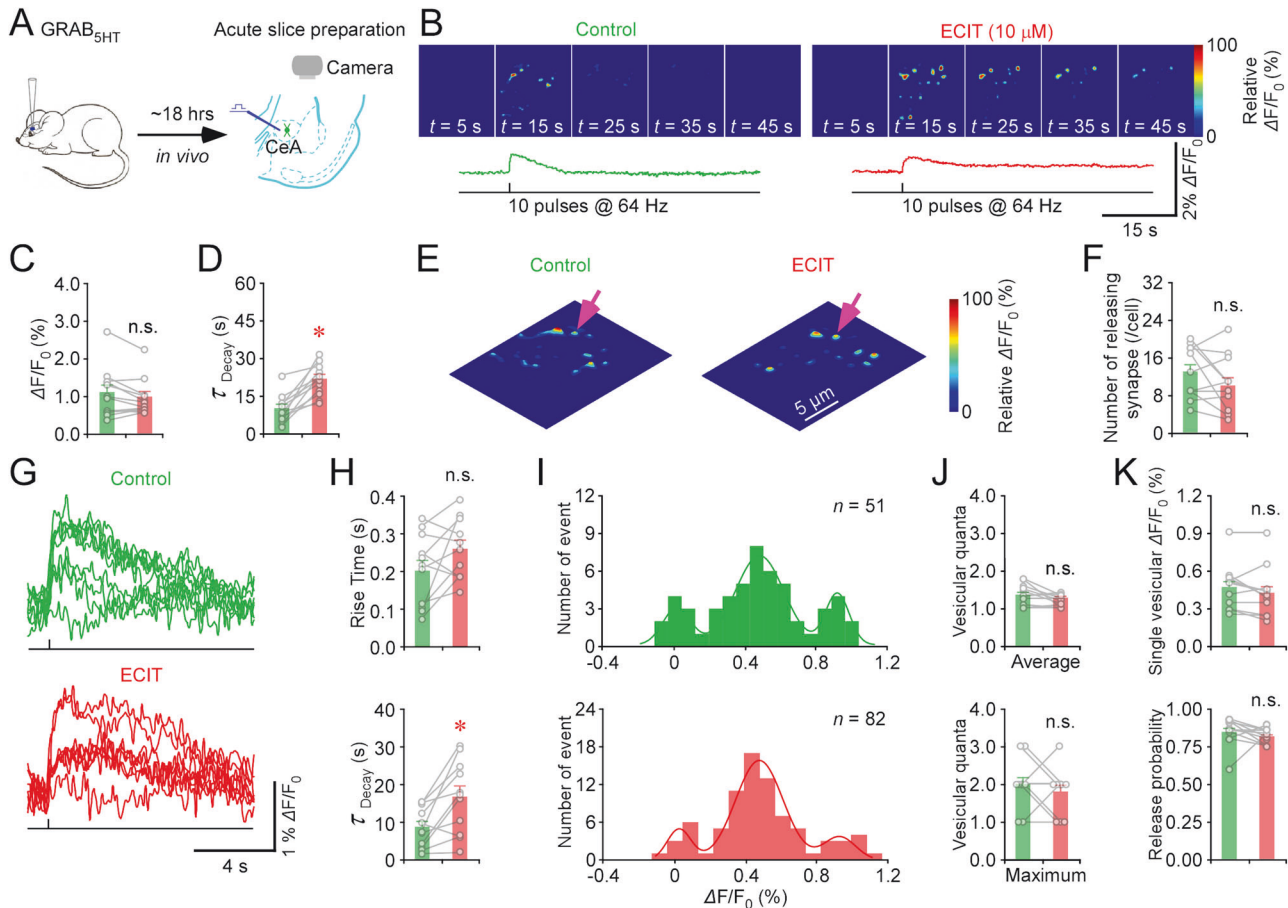
Fig. 4 Transporter inhibition prolongs amygdalar serotonin signals without affecting release. A Schematic of experiment design in a mouse amygdalar slice preparation. CeA: the central nucleus of the amygdala. **B** Heatmaps of electrically evoked fluorescence $\Delta F/F_0$ responses before (left) and after (right) the bath application of 10 μm escitalopram (**ECIT**) in the amygdala. **C–D** Peak amplitudes (Ctrl: 1.10 ± 0.19%; ECIT: 0.98 ± 0.14%, $Z = -1.41$, $p = 0.18$, $n = 12$ neurons from 6 animals) and decay time constants (Ctrl: 10.20 ± 1.59 s; ECIT: 21.97 ± 1.74 s, $Z = 3.06$, $p < 0.001$, $n = 12$ neurons from 6 animals) of GRAB$_{5HT}$ fluorescence $\Delta F/F_0$ responses before (green) and after (red) the bath application of ECIT. **E** 3D spatiotemporal profiling of electrically evoked fluorescence $\Delta F/F_0$ responses before (left) and after (right) the bath application of ECIT. Scale bars applied to all in **B** and **E**. **F** Releasing synapse counts before (green) and after (red) the bath application of ECIT (Ctrl: 13.09 ± 1.69; ECIT: 10.64 ± 1.76; $Z = -1.17$, $p = 0.28$, $n = 11$ neurons from 6 animals). **G** Ten $\Delta F/F_0$ responses evoked by single pulse stimuli at isolated releasing synapses before (green) and after (red) the bath application of ECIT. **H** 10–90% rise times (Ctrl: 0.21 ± 0.03 s; ECIT: 0.26 ± 0.02 s; $Z = 1.74$, $p = 0.08$; $n = 11$ neurons from 6 animals) and decay time constants (Ctrl: 8.61 ± 1.56; ECIT: 16.60 ± 2.83; $Z = 2.58$, $p = 0.01$; $n = 11$ neurons from 6 animals) of $\Delta F/F_0$ responses before (green) and after (red) the bath application of ECIT. **I** Amplitude histograms of $\Delta F/F_0$ responses before (green) and after (red) the bath application of ECIT. **J–K** Average (Ctrl: 1.37 ± 0.08; ECIT: 1.18 ± 0.05; $Z = -1.72$, $p = 0.10$, $n = 11$ neurons from 6 animals) and maximal (Ctrl: 2 ± 0.19; ECIT: 1.82 ± 0.18; $Z = -0.82$, $p = 0.56$, $n = 11$ neurons from 6 animals) vesicular quanta, quantal sizes (Ctrl: 0.47 ± 0.05%; ECIT: 0.43 ± 0.06%; $Z = -1.78$, $p = 0.08$, $n = 11$ neurons from 6 animals), and release probabilities (Ctrl: 84.59 ± 2.8%; ECIT: 81.70 ± 1.49%; $Z = -1.17$, $p = 0.27$, $n = 11$ neurons from 6 animals). Asterisks indicate $p < 0.05$ (Wilcoxon tests).

GRAB$_{5HT}$ in the amygdala of ePet-Cre mice, in which Cre recombinase is expressed under the serotonin transcription *FEV* promoter (Fig. S10A). Subsequently, we made optogenetic activation of serotonin fibers to induce selective release of serotonin at GRAB$_{5HT}$ expressing amygdalar neurons in the ex vivo amygdalar slice preparation. Escitalopram induced a similar transformation in the serotonin diffusion pattern released via optogenetic stimulation, without affecting the amount of serotonin released or the number of releasing synapses (Fig. S10; Movie S3). Collectively, these findings support the general role of serotonin transporters in regulating serotonin diffusion subsequent to its release.

Serotonergic transmission modes encode the properties of firing modes

The preceding data underscore the substantial impact of serotonin release and its interaction with transporters in serotonin signaling. This prompted our investigation to delve systematically

into how diverse modes of serotonergic transmission encode distinct characteristics of various firing modes within raphe serotonergic neurons (Fig. 7). As we increased the frequency of electric stimuli, we observed a corresponding escalation in evoked fluorescence $\Delta F/F_0$ responses, revealing a subtle positive linear relationship with the logarithmically scaled stimulation frequencies (Fig. 7A, B; Movie S4). Additionally, the evoked fluorescence $\Delta F/F_0$ responses of single releasing synapses showed a modest elevation with higher stimulation pulse numbers (Fig. 7A, B). These results align with the observed high release probability of serotonergic transmission. Moreover, the numbers of serotonin releasing synapses showed a robust correlation with the numbers of synchronously activated axons (Fig. 7C, D; Movie S5), uncovering an additional layer to the coding mechanism. Finally, the numbers of serotonin releasing synapses exhibited a weak positive correlation with stimulation frequencies, but not with pulse numbers (Fig. 7D), representing a third facet of the coding scheme. Taken together with the analysis of synaptic and volume
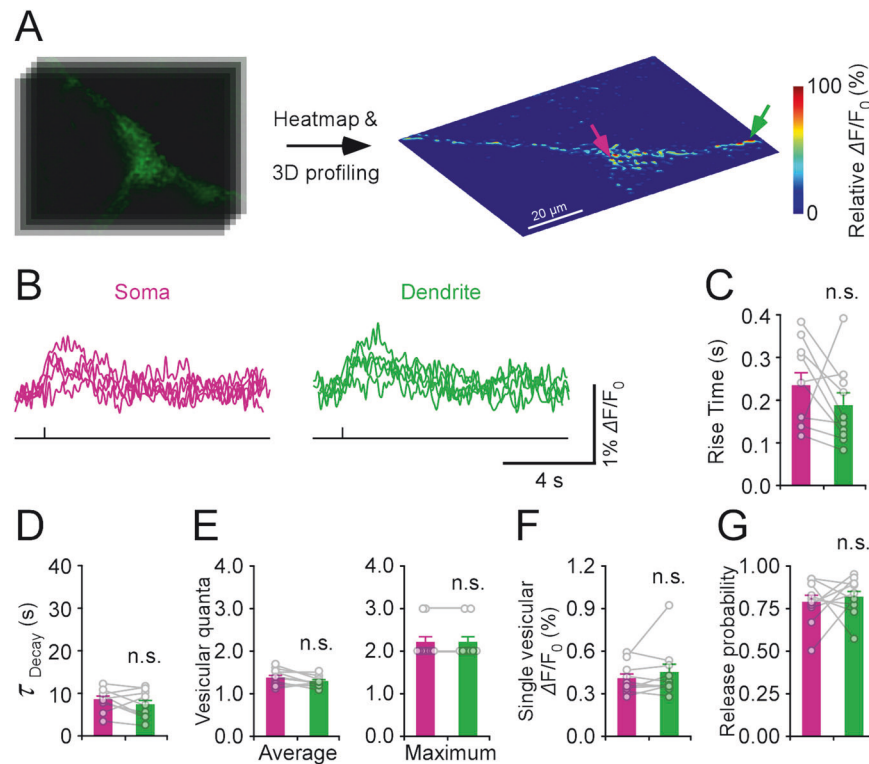
Fig. 5 Somatic and dendritic releasing synapses share the same properties. A Snapshots and 3D spatiotemporal profiling of electrically evoked fluorescence $\Delta F/F_0$ responses in the CeA. Note the isolated releasing synapses on the soma and dendrite indicated by pink and green arrows, respectively. **B** $\Delta F/F_0$ responses evoked by single pulse stimuli at isolated releasing synapses on the soma (pink) and dendrite (green). **C–D** 10–90% rise times (Soma: 0.24 ± 0.03 s; Dendrite: 0.19 ± 0.03 s; $U = 33.50$, $p = 0.23$) and decay time constants (Soma: 8.35 ± 0.81 s; Dendrite: 7.11 ± 1.00 s; $U = 40.00$, $p = 0.47$) of $\Delta F/F_0$ responses. **E–G** Average (Soma: 1.37 ± 0.06; Dendrite: 1.27 ± 0.04; $U = 33.00$, $p = 0.21$) and maximal (Soma: 2.20 ± 0.13; Dendrite: 2.20 ± 0.13; $U = 50.00$, $p = 0.96$) vesicular quanta, quantal sizes (Soma: $0.40 \pm 0.03\%$; Dendrite: $0.44 \pm 0.06\%$; $U = 56.50$, $p = 0.65$), and release probabilities (Soma: $78.00 \pm 4.00\%$; Dendrite: $81.40 \pm 3.47\%$; $U = 59.5$, $p = 0.50$) on the soma (green) and dendrite (cyan). Note n.s. indicates no statistical difference ($p > 0.05$; $n = 10$ neurons from 5 animals; Rank Sum non-parametric tests).

transmission, these results shed light on how serotonin utilizes neurotransmitter quantity and releasing synapse count to encode the frequency, number, and synchronicity of firing pulses, while employing additional volume transmission to signal heightened firing activities.

DISCUSSION

This study introduces a sensor-based imaging and FSCV method, enabling simultaneous recordings of synaptic, perisynaptic, proximate, and distal extrasynaptic serotonergic transmission for the first time. This method offers insights into the diverse modes and regulation of serotonin communication. Our key discovery highlights how various firing patterns of serotonergic neurons create distinct transmission modes. These transmission modes encode details about firing frequency, pulse number, and synchrony in neurotransmitter quantity, releasing synapse count, and the involvement of synaptic and/or volume transmission. These findings emphasize the intricate collaboration of synaptic structure, properties, and transporters in orchestrating the spectrum of serotonin transmission modes.

Serotonergic transmission modes

This study delineates a spectrum of serotonergic transmission modes. Serotonergic neurons participate in a wide array of behaviors, spanning cognition, mood, social interaction, sexual behavior, feeding behavior, motor behavior, reward, motivation, sleep-wake cycle, and thermoregulation [2, 3, 41]. Corresponding to this wide range of functions, serotonergic neurons exhibit a

diverse spectrum of firing patterns [4–9]. Yet, despite this connection, unraveling how these varied firing patterns impact serotonin release and signaling, subsequently influencing associated behaviors, has remained an enduring mystery [3, 10]. Here, we introduce an innovative method allowing for nanoscopic visualization of individual releasing synapses during transmitter release. Our analysis demonstrates that serotonergic neurons intricately encode the frequency, number, and synchronization of their firing pulses, converting these parameters into the quantity of serotonin released and the count of releasing synapses. Particularly noteworthy is the revelation that high-frequency and synchronized firing patterns overwhelm serotonin transporters, causing serotonin to disperse into the extracellular space and instigate volume transmission. Consequently, by modulating transmitter quantity, releasing synapse count, and employing synaptic and/or volume transmission, serotonergic neurons effectively convert diverse firing modes into distinct intercellular signals. The complexity of these signals has the potential to transmit heterogeneous firing patterns to varied spatiotemporally defined G-protein coupled receptor signaling in postsynaptic targets, initiating a broad range of functions [42, 43].

Conversion of synaptic to volume transmission via channeled diffusion

Our analysis offers new insights into another enduring debate on serotonergic transmission. The prevailing volume transmission theory posits that neuromodulatory transmitters, like serotonin, diffuse extensively across long distances, influencing various nearby cells [12, 13]. However, this theory relies on the assumption
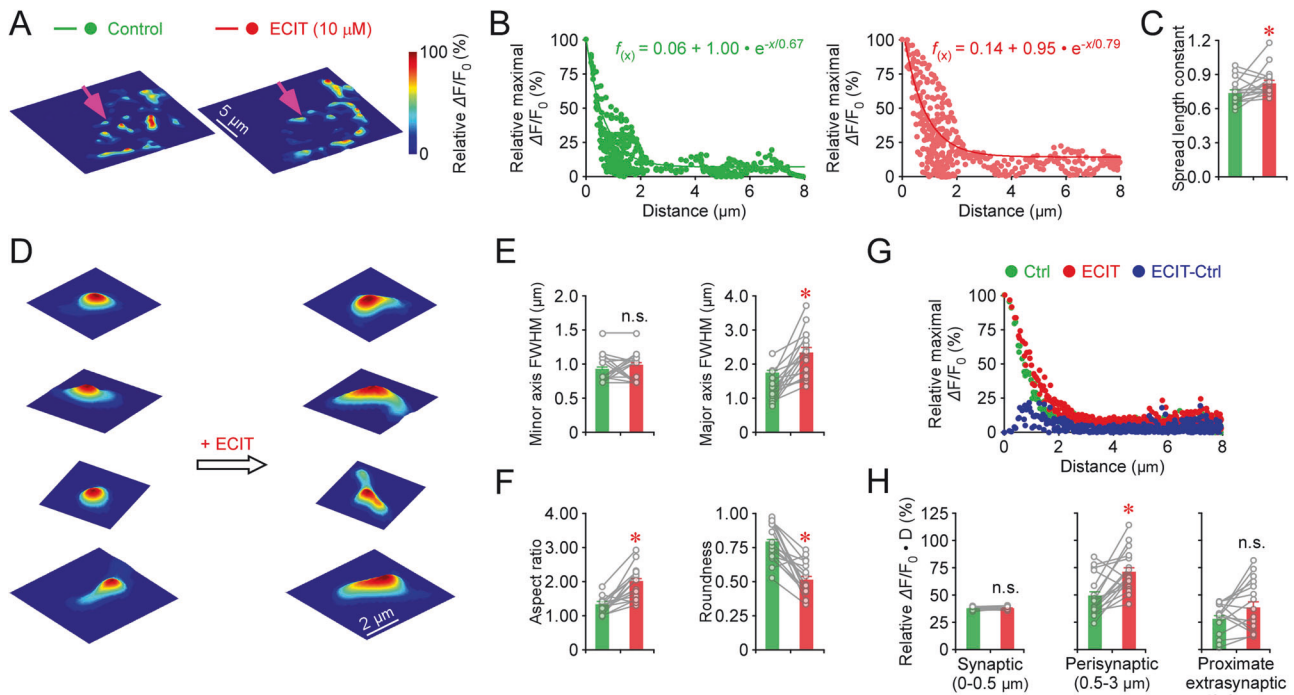
Fig. 6 Transporter inhibition drives extrasynaptic diffusion of serotonin. A 3D spatiotemporal profiling of electrically evoked fluorescence $\Delta F/F_0$ responses before (left) and after (right) the bath application of 10 μm escitalopram (**ECIT**). **B** Pixel-wise maximal $\Delta F/F_0$ plots before (left) and after (right) the bath application of ECIT at the same isolated release site indicated by the pink arrows in **A**. **C** Averaged spatial spread length constants (Ctrl: 0.72 ± 0.03 μm; ECIT: 0.84 ± 0.04 μm, $Z = 2.67$, $p = 0.007$, $n = 17$ releasing synapses from 5 animals). **D** 3D profiling of $\Delta F/F_0$ responses at isolated releasing synapses before and after the bath application of ECIT. Note serotonin leaking out of synapses via $1-3$ outlets after the bath application of ECIT (1.53 ± 0.17; $n = 17$ releasing synapses from 5 animals). Scale bar applied to all in **D**. **E** Minor (Ctrl: 0.93 ± 0.05 μm; ECIT: 0.98 ± 0.05 μm; $Z = 0.59$, $p = 0.58$, $n = 17$ releasing synapses from 5 animals) and major (Ctrl: 1.31 ± 0.10 μm; ECIT: 2.32 ± 0.16 μm; $Z = 3.62$, $p < 0.001$, $n = 17$ releasing synapses from 5 animals) full width at half maximums (**FWHMs**) of serotonin diffusion profiles at isolated releasing synapses before and after the bath application of ECIT. **F** Aspect ratio (Ctrl: 1.30 ± 0.06; ECIT: 2.02 ± 0.11; $Z = 3.48$, $p < 0.001$, $n = 17$ releasing synapses from 5 animals) and roundness (Ctrl: 0.79 ± 0.03; ECIT: 0.52 ± 0.03; $Z = -3.53$, $p < 0.001$, $n = 17$ releasing synapses from 5 animals) values of serotonin diffusion profiles at isolated releasing synapses before and after the bath application of ECIT. **G** Plots of pixel-wise maximal $\Delta F/F_0$ before (green) and after (red) the bath application of ECIT and their difference (cyan; ECIT-Ctrl). **H** Relative integration values of $\Delta F/F_0$ at distance of 0.5 μm (Ctrl: 0.37 ± 0.003; ECIT: 0.38 ± 0.003; $Z = 1.34$, $p = 0.19$, $n = 17$ releasing synapses from 5 animals), $0.5 - 3$ μm (Ctrl: 0.49 ± 0.04; ECIT: 0.71 ± 0.05; $Z = 2.91$, $p = 0.002$, $n = 17$ releasing synapses from 5 animals), and $3 - 8$ μm (Ctrl: 0.27 ± 0.04; ECIT: 0.38 ± 0.06; $Z = 1.91$, $p = 0.06$, $n = 17$ releasing synapses from 5 animals). Asterisks indicate $p < 0.05$ (Wilcoxon tests).

that endogenously released neuromodulators behave akin to exogenously applied ones, freely diffusing in the extrasynaptic space—an assumption lacking direct experimental support [44, 45]. Recent studies employing improved voltammetry challenge this view, suggesting a serotonin diffusion range of ~20 μm or slightly more, resembling paracrine-like transmission [46, 47]. Nonetheless, due to voltammetry's limitations in measuring solely extracellular serotonin, these studies do not have spatial resolution to directly examine serotonergic transmission at synapses [11]. Conversely, an electrophysiology study suggests that serotonergic transmission primarily occurs via synaptic mechanism with minimal crosstalk between synapses [14]. However, this study, reliant on indirect analysis, struggles to explain observed evidence supporting serotonin spillover in some experiments. Here, our imaging analysis presents the first nanoscopic visualization of highly confined diffusion of serotonin at individual releasing synapses, supporting the presence of tightly restricted synaptic serotonergic transmission as a typical mode of signaling, with volume transmission occurring under specialized conditions [34].

In this study, our comprehensive high-resolution imaging analysis reveals serotonin's diffusion dynamics. At synapses, serotonin diffuses freely in a distinctive cone-shaped pattern within a radius of ~0.5 μm from the release site. However, at perisynaptic and proximate extrasynaptic regions, serotonin is rapidly cleared by transporters, causing a steep concentration

drop, often leaving only a minimal concentration undetectable by $FSCV_{5HT}$ at distal extrasynaptic sites. During heightened release or under transporter inhibition, a slightly larger quantity manages to escape synapses through one, sometimes two, or occasionally three outlets. While this increased release remains below $GRAB_{5HT}$ detection threshold at proximate extrasynaptic sites, it becomes detectable at distal extrasynaptic sites by $FSCV_{5HT}$. This hints a volume transmission, mediated for example by the high affinity serotonin receptors expressed in certain brain areas [48]. The outlets exposed to transporter inhibition suggest the existence of channeled synaptic enclosures. This is consistent with ultra-structural observations of numerous clusters of curved gap junctions, which form annular or tapered annular profiles with diameters ranging from ~2–7 μm at serotonergic perisynaptic sites [39, 49]. These channeled synaptic enclosures likely play a significant role in dispersing serotonin into extracellular sites, particularly by governing the diffusion direction of serotonin via 1–3 exiting channels. Nevertheless, owing to the spatial resolution limitations of $FSCV_{5HT}$, it remains to determine whether serotonin diffuses freely or through specific channels that are physically restricted by cellular structures and/or regulated by transporters (see [40]) at the distal extracellular space.

Based on the serotonin concentration-fluorescence response curve obtained from the perfusion experiment, we estimated that ~100 nM of serotonin is released per quantal event. At these concentrations, fewer than one serotonin molecule would be
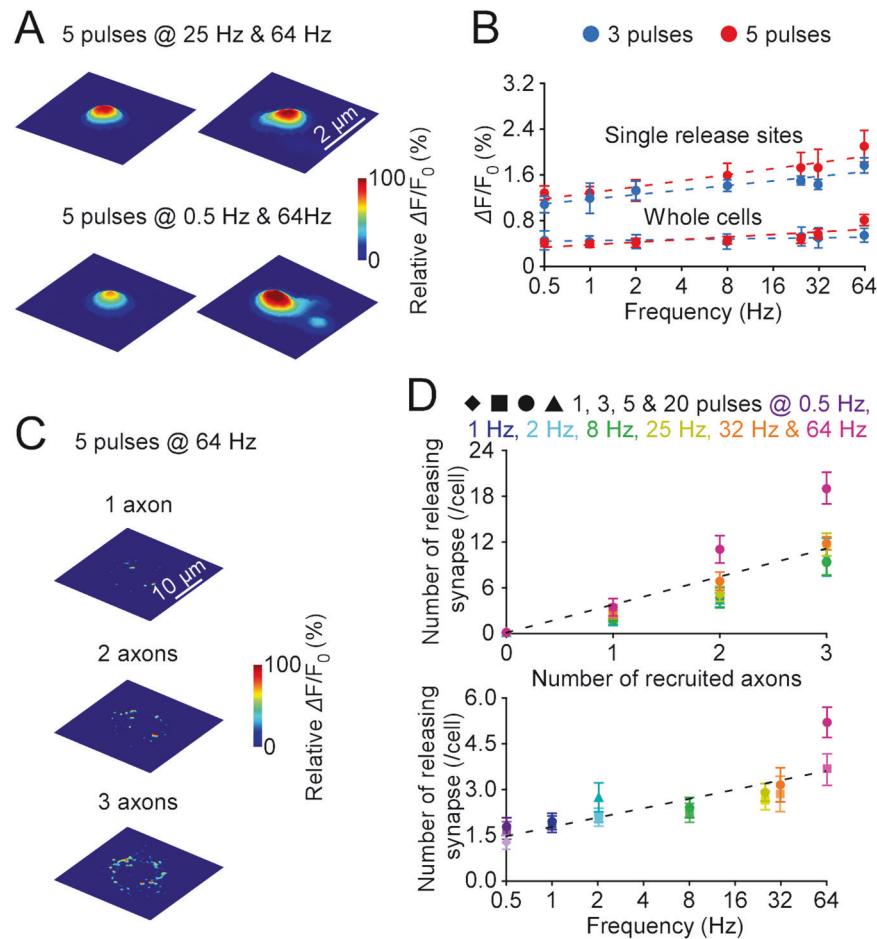
Fig. 7 Serotonin release properties encode frequency, number, and synchrony of firing pulses. A Heatmaps of fluorescence $\Delta F/F_0$ responses electrically evoked by 5-pulse stimuli delivered at varied frequencies. Scale bars applied to all in **A**. **B** Plots of whole-cell and single releasing synapse maximal fluorescence $\Delta F/F_0$ responses against frequencies of stimuli containing 3 pulses (Whole cell: 0.5 Hz: $0.49 \pm 0.15\%$; 1 Hz: $0.47 \pm 0.09\%$; 2 Hz: $0.46 \pm 0.12\%$; 8 Hz: $0.46 \pm 0.13\%$; 25 Hz: $0.54 \pm 0.17\%$; 32 Hz: $0.53 \pm 0.18\%$; 64 Hz: $0.57 \pm 0.13\%$, $n = 5$ neurons from 3 animals, fitted with log functions $f_{(x)} = 0.47 + 0.013 \cdot \mathrm{Log}_2 (x)$ ($r^2 = 0.60$, $F = 7.55$, $p = 0.04$); Single releasing synapse: 0.5 Hz: $1.11 \pm 0.15\%$; 1 Hz: $1.23 \pm 0.26\%$; 2 Hz: $1.35 \pm 0.16\%$; 8 Hz: $1.43 \pm 0.10\%$; 25 Hz: $1.52 \pm 0.08\%$; 32 Hz: $1.47 \pm 0.09\%$; 64 Hz: $1.79 \pm 0.13\%$, $n = 5$ releasing synapses from 3 animals, fitted with log functions $f_{(x)} = 1.21 + 0.08 \cdot \mathrm{Log}_2 (x)$ ($r^2 = 0.87$, $F = 33.64$, $p = 0.002$)) and 5 pulses (Whole cell: 0.5 Hz: $0.40 \pm 0.07\%$; 1 Hz: $0.38 \pm 0.06\%$; 2 Hz: $0.41 \pm 0.08\%$; 8 Hz: $0.44 \pm 0.07\%$; 25 Hz: $0.46 \pm 0.08\%$; 32 Hz: $0.55 \pm 0.09\%$; 64 Hz: $0.80 \pm 0.10\%$, $n = 9$ neurons from 5 animals, fitted with log functions $f_{(x)} = 0.38 + 0.042 \cdot \mathrm{Log}_2 (x)$ ($r^2 = 0.78$, $F = 7.57$, $p = 0.04$); Single releasing synapse: 0.5 Hz: $1.29 \pm 0.11\%$; 1 Hz: $1.29 \pm 0.11\%$; 2 Hz: $1.33 \pm 0.18\%$; 8 Hz: $1.58 \pm 0.20\%$; 25 Hz: $1.73 \pm 0.26\%$; 32 Hz: $1.71 \pm 0.32\%$; 64 Hz: $2.09 \pm 0.27\%$, $n = 9$ releasing synapses from 5 animals, fitted with log functions $f_{(x)} = 1.30 + 0.10 \cdot \mathrm{Log}_2 (x)$ ($r^2 = 0.89$, $F = 39.53$, $p = 0.002$)). **C** Heatmaps of stepwise fluorescence $\Delta F/F_0$ responses electrically evoked by 5-pulse stimuli delivered at varied voltage intensities. Note the difference in number of releasing synapses in step 1–3 fluorescence $\Delta F/F_0$ responses. Scale bars applied to all in **C**. **D** Upper, plot correlating numbers of releasing synapses with presumably recruited axons. Note the correlation fitting with a linear function of $f_{(x)} = 3.68 \cdot x$ ($r^2 = 0.95$, $F = 53.23$, $p < 0.05$). Lower, plot of numbers of releasing synapses against 1-, 3-, 5-, and 20-pulse stimuli delivered at 0.5 Hz (1 pulse: 1.30 ± 0.21, $n = 5$ from 3 animals; 3 pulses: 1.60 ± 0.40, $n = 5$ from 3 animals, 5 pulses: 1.77 ± 0.28, $n = 9$ from 5 animals), 1 Hz (3 pulses: 1.80 ± 0.2, $n = 5$ from 3 animals; 5 pulses: 1.92 ± 0.26, $n = 9$ from 5 animals), 2 Hz (3 pulses: 2.00 ± 0.45, $n = 5$ from 3 animals; 5 pulses: 2.15 ± 0.22, $n = 9$ from 5 animals; 20 pulses: 2.72 ± 0.48, $n = 9$ from 5 animals), 8 Hz (3 pulses: 2.20 ± 0.37, $n = 5$ from 3 animals; 5 pulses: 2.39 ± 0.31, $n = 9$ from 5 animals), 25 Hz (3 pulses: 2.60 ± 0.40, $n = 5$ from 3 animals; 5 pulses: 2.88 ± 0.30, $n = 9$ from 5 animals), 32 Hz (3 pulses: 2.80 ± 0.37, $n = 5$ from 3 animals; 5 pulses: 3.10 ± 0.56, $n = 10$ from 5 animals), 64 Hz (3 pulses: 3.60 ± 0.40, $n = 5$ from 3 animals; 5 pulses: 5.16 ± 0.50, $n = 10$ from 5 animals), fitted with a linear function of $f_{(x)} = 0.31 \cdot x + 1.75$ ($r^2 = 0.79$, $F = 18.62$, $p < 0.01$).

present in the cleft volume of serotonergic synapses (~0.6–0.8 μm in diameter; [50–52]), which seems implausible. Previous studies suggest that serotonin 2C receptors may exhibit ~25–50 times lower affinity at synapses [37, 53, 54]. Since synaptic GRAB$_{5HT}$ sensors share similar pharmacological properties with serotonin 2C receptors [55], their affinity at synapses may also be significantly reduced. Consequently, synaptic serotonin concentrations might be underestimated by a similar factor, implying that ~2.5–5 mM of serotonin could be released per quantal event. Directly measuring the synaptically evoked serotonin concentration-fluorescence response, as previously demonstrated by Marcott and colleagues [56], is essential for accurately

calibrating the vesicular quantal size and validating this study's main conclusions.

Biological and clinical implication

Intercellular communication, which is mediated by *fast*-acting transmitters glutamate and gamma-aminobutyric acid (**GABA**), and by hundreds (>500) of *slow*-acting neuromodulatory transmitters (e.g., monoamines, neuropeptides, and other molecules), orchestrates diverse behavioral and physiological processes [57, 58]. A wealth of knowledge has been acquired thanks to the remarkable sensitivity and temporal resolution of electrophysiological recordings, as well as through Herculean

experiments examining fast neurotransmitters [59–61]. It is worth noting that in the early 1990s, the advent of high-resolution patch-clamp recordings enabled the quantitative analysis of glutamatergic and GABAergic synaptic transmissions and their properties [62–64]. The technique sparked a significant wave of discoveries concerning synaptic transmission and plasticity. These breakthroughs include silent synapses, synaptic receptor trafficking, synaptic molecular signaling, synaptic nanocolumnar organization, and many other vital insights crucial for comprehending the brain, body, associated disorders, and ultimately, for identifying pathogenic mechanisms and therapeutic strategies [58, 65–67]. Unfortunately, patch-clamp recordings fall short in effectively capturing neuromodulatory transmission properties. Other methods, like microdialysis and voltammetry, despite many recent improvements, still lack vital spatial and/or temporal resolution [11]. Therefore, despite extensive research linking slow-acting neuromodulatory transmitters to diverse physiological actions and diseases, a significant gap persists, hindering comprehensive understanding of neuromodulatory regulation and function. The emergence of genetically encoded fluorescence sensors, many of which emit abundant photons, presents a promising avenue. Our theoretical groundwork suggests that employing image analysis algorithms could potentially convert the surplus collected photons into enhanced spatial and temporal resolution, offering a means to decode neuromodulatory transmission [68, 69].

Recently developed image analysis program, GESIAP, has demonstrated its utility in delineating fundamental synaptic properties at individual serotonin releasing synapses [31, 35]. This includes aspects like transmitter spatial diffusion, quantal size, quantal content, release probability, pool size, and refilling rate. Here, we show the ability of GESIAP to enable nanoscopic visualization of serotonin diffusion across various behavior-related activity patterns. This reveals how channeled synaptic enclosures, synaptic properties, and transporters collaboratively shape serotonergic transmission modes. This mechanism explains why SSRIs may elevate extracellular serotonin levels, as observed in voltammetry [18–21], without affecting serotonin release at synapses. More importantly, the findings predict that the alterations in serotonin transporters, whether they occur due to physiological, pathological, or clinical conditions (e.g., see [1, 70]; see also [41]), as well as changes in synaptic structure and properties (our unpublished data), hold the potential to influence behaviors and contribute to the development and prognosis of various diseases. We observe that fundamental synaptic properties of serotonergic transmission are largely conserved across different brain areas (e.g., the thalamic geniculate, dentate gyrus, dorsal raphe, and amygdala), animal species (e.g., mouse, rat, and human), and preparations (e.g., cultured neuron systems, ex vivo, and intact brains) (this study; [31, 34]; our unpublished data). Therefore, the method reported herein, which enables effective quantification of synaptic changes and transporter functions, promises to provide insights into synaptic mechanisms involved in a range of serotonin-linked diseases, e.g., major depressive disorders, digestive disorder, obsessive-compulsive disorder, sexual dysfunction, sleep disorder, and social anxiety disorder [1–3].

METHODS
Animal preparations
Wild type C57BL/6J mice (Jackson Laboratory, Bar Harbor, ME; RRID:IMSR_-JAX:000664), ePet-Cre mice (Jackson Laboratory; Stock #012712; RRID:IMSR_JAX:012712) bred congenically on the C57BL/6J background [71], and Sprague Dawley rats were utilized in this study. Genotyping was conducted through standard PCR using genomic DNA extracted from tail samples, employing transgene primers: 5′-GCG GTC TGG CAG TAA AAA CTA TC-3′ (Forward) and 5′-GTG AAA CAG CAT TGC TGT CAC TT-3′ (Reverse), and internal positive control primers 5′-CTA GGC CAC AGA ATT

GAA AGA TCT-3′ (Forward) and 5′-GTA GGT GGA AAT TCT AGC CAT CAT C-3′ (Reverse). Heterozygous ePet-Cre mice exhibiting specific DNA bands at both transgene and internal positive control positions were included in the experiments.

Both male and female animals were included and neither genetically encoded sensor-based imaging nor fast-scan cyclic voltammetry (**FSCV**) detected any difference in serotonergic responses measured in tissues prepared from males versus females. Animals were maintained in the animal facility at the University of Virginia and family- or pair-housed in the temperature-controlled animal room with 12-h/12-h light/dark cycle. Food and water were available *ad libitum*. All procedures for animal and human cell line experiments were performed following protocols (No. 3168) approved by the Animal Care & Use Committee of the University of Virginia and in accordance with US National Institutes of Health guidelines.

Cultured and acute slice preparations
Organotypic hippocampal cultured slices were prepared from postnatal 5–7 day old male/female Sprague Dawley rats, following our previous studies [72]. Briefly, the hippocampi were dissected out in ice-cold HEPES-buffered Hanks' solution (pH 7.35) under sterile conditions, sectioned into 400 µm slices on a tissue chopper, and explanted onto a Millicell-CM membrane (0.4-µm pore size; Millipore, Billerica, MA). The membranes were then placed in 750 µl of MEM culture medium, contained (in mM): HEPES 30, heat-inactivated horse serum 20%, glutamine 1.4, D-glucose 16.25, NaHCO$_3$ 5, CaCl$_2$ 1, MgSO$_4$ 2, insulin 1 mg/ml, ascorbic acid 0.012% at pH 7.28 and osmolarity 320. Cultured slices were maintained at 35 °C, in a humidified incubator ambient air enriched with 5% CO$_2$.

Acute dorsal raphe and amygdalar slices were typically prepared from P42 − 60 male/female C57BL/6 J mice ~18 h after in vivo viral expression of genetically encoded serotonin sensor as our previous reports [25, 31]. Animals were deeply anesthetized by xylazine-ketamine and decapitated. The brain containing the dorsal raphe nucleus or the amygdala or the central nucleus of the amygdala was quickly removed and placed into cold (0–4 °C) oxygenated physiological solution containing (in mM): NaCl 125, KCl 2.5, NaH$_2$PO$_4$ 1.25, NaHCO$_3$ 25, MgCl$_2$ 1, dextrose 25, and CaCl$_2$ 2, pH 7.4. Coronal slices 350 µm thick were cut from the brain blocks. These slices were kept at 37.0 ± 0.5 °C in oxygenated physiological solution for ~0.5–1 h before sensor imaging and FSCV recordings.

During imaging and FSCV recordings, the brain slices were submerged in a chamber and stabilized with a fine nylon net attached to a platinum ring. The recording chamber was perfused with oxygenated physiological solution. The half-time for the bath solution exchange was ~6 s, and the temperature of the bath solution was maintained at 34.0 ± 0.5 °C. All antagonists were bath-applied.

GRAB$_{5HT}$ preparation and expression
Genetically encoded serotonin fluorescent sensors GRAB$_{5HT1.0}$ and iSeroSnFR were sub-cloned into Sindbis viral vector pSinREP5 with Xba1 and Sph1 restriction digestion, and viral particles were produced and expressed following our previous studies [25, 27]. For in vitro sensor expression, a glass pipette was used to deliver ~10 nl of Sindbis solution by pressure injection to infect CA1 pyramidal neurons in cultured hippocampal slices. Experiments were typically performed within 18 ± 4 h of Sindbis viral infection.

For in vivo sensor expression, animals were initially anesthetized by an intraperitoneal injection of ketamine and xylazine (10 and 2 mg/kg, respectively), and then placed in a stereotaxic frame. A glass pipette was used to penetrate the dorsal raphe nucleus (**DR**) and the central nucleus of the amygdala (**CeA**) according to stereotaxic coordinates (DR: AP −4.35 mm, ML: 0.00 mm, DV: −3.20 mm; CeA: AP −1.50 mm, ML: ±2.50 mm, DV: −4.70 mm) to deliver ~50 nl of Sindbis solution by pressure injection to infect raphe neurons. For in vivo opsin expression, 80 nl of AAV-Syn-FLEX-ChrimsonR-tdTomato viral solution (Addgene, Watertown, MA; RRID:Addgene_62723) was injected into DR of ePet-Cre mice. The in vivo viral injection micropipette was typically left in the brain for ~10 min after the injection to ensure proper viral diffusion. Experiments were typically conducted within 18 ± 4 h after Sindbis viral infection and 5–6 weeks after AAV viral infection to achieve optimal expression [73, 74].

Electric and optogenetic activation of serotonin release
Serotonin release was triggered using either electrical or optogenetic approaches. To evoke serotonergic responses through electrical stimulation, a bipolar cluster stimulating electrode (CE2C65; FHC, Bowdoin, ME)

was typically employed and positioned near either the dorsal raphe nucleus or the amygdala. The stimulation current varied between ~100–350 μA, with each pulse lasting 1 ms. Except in the case of minimal stimulation experiments designed to evaluate the incremental recruitment of activated axons, suprathreshold stimulation was typically administered to ensure the activation of serotonergic fibers, as confirmed by consistent whole-cell fluorescence responses. The evoked fluorescence responses were sensitive to bath application of TTX, 0 mM Ca^{2+}/10 mM Mg^{2+}, calcium channel blockers, and pharmacological inhibitors of sensors (Fig. S3; see also [25, 27, 28, 31, 33, 34]), confirming synaptic responses.

To optogenetically induce serotonin release, a 200 μm diameter optical fiber (Thorlabs, Newton, NJ) was positioned near CeA along the serotonergic fiber pathway to activate ChrimsonR (Cre-dependent) using a 635-nm laser (Opto Engine LLC, Midvale, UT). The stimulation protocol consisted of five pulses, each lasting 10 ms, delivered at 64 Hz, with the light intensity set to 10 mW/mm² at the fiber tip. Additionally, 200 μM 4-AP was included into the bath solution to facilitate optogenetic activation. Moreover, to prevent unintended opsin activation during the simultaneous GRAB$_{5HT}$ sensor-based imaging, a low sensor excitation light intensity of 0.07 mW/mm² was typically used in these experiments. Furthermore, due to the high power required for optogenetic activation, only low frequency and low intensity stimulation was applied in this study. To avoid interference of the optogenetic excitation light with GRAB$_{5HT}$ fluorescence responses, 2–3 frames of images obtained during optogenetic stimulation were excluded from the analysis.

Sensor-based functional imaging
Due to the slow nature of neuromodulatory transmission, long-term imaging (from seconds to minutes) became necessary to capture the action of transmitters and resolve their properties. To minimize drift and fluctuation vital for high-resolution visualization of transmitter release-induced fluorescence responses [68], a stable recording/stimulation and imaging setup was used to carry out all imaging and FSCV recording experiments [33, 75]. Wide-field epifluorescence imaging was performed using a Hamamatsu ORCA FLASH4.0 camera (Hamamatsu Photonics, Shizuka, Japan), and fluorescent sensor expressing cells in acutely prepared tissue slices were excited by a 460-nm ultrahigh-power low-noise LED (Prizmatix, Givat-Shmuel, Israel) [27, 75]. The frame rate of the FLASH4.0 camera was set to 10–50 Hz. Fluorescence signals were collected with an Olympus 40× water-immersion objective with a numerical aperture of 0.8. Despite variable fluorescence F_0 across the entire cell membrane surface of neurons due to heterogeneous GRAB$_{5HT}$ sensor expression, the $\Delta F/F_0$ responses showed no or weak correlation with the basal fluorescence F_0, suggesting independence from sensor expression levels and reliability in measuring transmitter concentration (Fig. S11; cf. [31, 34]).

Imaging analysis with GESIAP
Recent advancements in computational algorithms technology have spurred a swift expansion of applications for superresolution wide-field deconvolution microscopy [76–79], which can achieve ~150–200 nm spatial resolution, sufficient to resolving synapses, including serotonergic synapses sizing ~0.6–0.8 μm in diameters [50–52]. We have previously validated its applicability in sensor-based functional imaging, both theoretically [68] and experimentally [34]. In this study, fluorescence responses were analyzed using enhanced algorithms derived from our recently created genetically encoded sensor-based image analysis program (**GESIAP**) [31]. The improved program (i.e., GESIAP3.0 codes [35], generously shared by Ke Si, Jiazhu Zhu, and Roger R. Zhu, Zhejiang University) proved to be was effective in extracting small fluorescence responses from individual releasing synapses [68], essential for delineating synaptic properties. The algorithms were created using MATLAB 2023a with MATLAB's Image Processing Toolbox (Mathworks, Natick, MA). The fluorescence response traces typically represented the whole-cell average responses of individual neuronal somata of interest, unless stated otherwise (e.g., single releasing synapses on the soma and dendrite). To visualize individual transmitter releasing synapses and estimate post-synaptic transmitter diffusion extent, the maximal electrically evoked maximal $\Delta F/F_0$ responses at individual pixels over time were plotted to create 3D spatial profiles for individual releasing synapses. Pixels with the maximal $\Delta F/F_0$ responses in individual releasing synapses were assumed to be the centers of release. Fluorescence $\Delta F/F_0$ intensity profiles at well-isolated releasing synapses were fit with a single-exponential decay function, and their decay constants were extracted as the spatial spread length constants. We found that higher-order decay functions, such as

two-exponential decay functions, provided only limited improvement in fitting both the control and SSRI conditions, and therefore opted for one-exponential fits for simplicity. To estimate the quantal properties of individual transmitter releases, 20-pulse trains at low frequency (0.1 Hz) were used to evoke transmitter release. The evoked fluorescence responses at isolated individual releasing synapses were fit with a double-exponential synaptic function incorporating the response properties of GRAB$_{5HT}$, using MATLAB algorithms in GESIAP generously shared by Roger R. Zhu [34, 35]. This provided estimates of key parameters of the evoked events such as rise time, decay time constant, and amplitude. The quantal properties, such as quantal content, quantal size, and release probability, were determined using the classic quantal analysis approach [62–64].

Fast-scan cyclic voltammetry
Carbon-fiber microelectrodes (**CFME**) were fabricated from 7 μm T-650 carbon fibers (Cytec Engineering Materials Inc, Tempe, AZ), which were aspirated into a glass capillary (1.2 mm OD and 0.68 mm ID, A-M System, Sequim, WA) and pulled into electrodes with a PE-22 puller (Narishige International USA Inc, Amityville, NY). The carbon fiber was trimmed to 50 to 70 μm in length from the pulled glass tip, and then sealed with Epon epoxy cured at 100 °C for 2 h followed by 150 °C overnight. CFMEs were cleaned in isopropyl alcohol for 30 min, and then electrochemically deposited by submerging CFME tip in Nafion® solution (5 wt% 1100 EW Nafion® in methanol, Ion Power, New Castle, DE) with a constant potential of 1.0 V vs Ag/AgCl applied to them for 30 s [80]. The Nafion-coated electrodes were air-dried for 10 s, and then at 70 °C for 10 min. For electrochemical detection of 5HT, a Jackson waveform was applied to the electrode by scanning the potential cycling from $0.2 \rightarrow 1.0 \rightarrow -0.1 \rightarrow 0.2$ V at 1000 V/s using a Dagan ChemClamp potentiostat (Pine Research Instrumentation, Durham, NC). Due to the potential eletrode fouling [81], the observed enhanced FSCV$_{5HT}$ responses might be understimated in the presenece of SSRIs. For data collection and analysis, TarHeel CV (generously provided by R. Mark Wightman, University of North Carolina) was used. For the electrode calibrations, phosphate buffer solution was used which consisting of (in mM): NaCl 131.25, KCl 3.0, NaH$_2$PO$_4$ 10.0, MgCl$_2$ 1.2, Na$_2$SO$_4$ 2.0, and CaCl$_2$ 1.2, at pH 7.4. A serotonin stock solution was prepared in 0.1 M HClO$_4$ and diluted to 500 nM with phosphate buffer solution for calibrations prior to the experiment.

Experimental operation and data collection
The experiments were operated under control of a single custom-written program based on IGOR (WaveMetrics, Lake Oswego, OR) for electro-physiology, optogenetics, and functional imaging [75, 82]. This program synchronized image capture, voltammetry, electric or optogenetic stimulations, and comprehensive data collection. The voltammetric FSCV$_{5HT}$ response recording started typically 10 s after GRAB$_{5HT}$ imaging to avoid the potential blue light-induced photoelectric effect on the measurement of evoked voltammetric responses [83].

Statistical analysis
Statistical results were reported as mean±s.e.m. Animals or cells were randomly assigned into control or experimental groups and investigators were blinded to experimental treatments. Based on the effect size d calculated from previous and preliminary data, the sample size is estimated to be ≥~8–25/group to attain the desired power of ≥80% with statistical significance set as $\alpha < 0.05$. Statistical significance of the means is determined using Wilcoxon and Mann-Whitney Rank Sum non-parametric tests for paired and unpaired samples, respectively. Statistical significance of the relationship of two data groups is determined using regression t test provided the normality and constant variance tests passed. The data that support the findings of this study are available from the corresponding authors upon request.

DATA AVAILABILITY
The authors confirm that the data supporting the findings of this study are available within the article and its supplementary materials. All relevant data have been presented in this article. There was no data excluded from the analysis.

REFERENCES

1. Marx W, Penninx B, Solmi M, Furukawa TA, Firth J, Carvalho AF, et al. Major depressive disorder. Nat Rev Dis Primers. 2023;9:44.
2. Beyeler A, Ju A, Chagraoui A, Cuvelle L, Teixeira M, Di Giovanni G, et al. Multiple facets of serotonergic modulation. Prog BraRes. 2021;261:3–39.
3. Okaty BW, Commons KG, Dymecki SM. Embracing diversity in the 5-HT neuronal system. Nat Rev Neurosci. 2019;20:397–424.
4. Li Y, Zhong W, Wang D, Feng Q, Liu Z, Zhou J, et al. Serotonin neurons in the dorsal raphe nucleus encode reward signals. Nat Commun. 2016;7:10503.
5. Cohen JY, Amoroso MW, Uchida N. Serotonergic neurons signal reward and punishment on multiple timescales. eLife. 2015;4:e06346. https://doi.org/10.07554/eLife.06346.
6. Nakamura K, Matsumoto M, Hikosaka O. Reward-dependent modulation of neuronal activity in the primate dorsal raphe nucleus. J Neurosci. 2008;28:5331–43.
7. Hayashi K, Nakao K, Nakamura K. Appetitive and aversive information coding in the primate dorsal raphe nucleus. J Neurosci. 2015;35:6195–208.
8. Liu Z, Zhou J, Li Y, Hu F, Lu Y, Ma M, et al. Dorsal raphe neurons signal reward through 5-HT and glutamate. Neuron. 2014;81:1360–74.
9. Miyazaki K, Miyazaki KW, Doya K. Activation of dorsal raphe serotonin neurons underlies waiting for delayed rewards. J Neurosci. 2011;31:469–79.
10. Ligneul R, Mainen ZF. Serotonin. Curr Biology: CB. 2023;33:R1216–R1221.
11. Muir J, Anguiano M, Kim CJS. Neuromodulator and neuropeptide sensors and probes for precise circuit interrogation in vivo. Science. 2024;385:eadn6671.
12. Agnati LF, Bjelke B, Fuxe K. Volume transmission in the brain. Am Sci. 1992;80:362–73.
13. Zoli M, Jansson A, Sykova E, Agnati LF, Fuxe K. Volume transmission in the CNS and its relevance for neuropsychopharmacology. Trends Pharmacol Sci. 1999;20:142–50.
14. Courtney NA, Ford CP. Mechanisms of 5-HT1A receptor-mediated transmission in dorsal raphe serotonin neurons. J Physiol. 2016;594:953–65.
15. Murphy SE, Capitao LP, Giles SLC, Cowen PJ, Stringaris A, Harmer CJ. The knowns and unknowns of SSRI treatment in young people with depression and anxiety: efficacy, predictors, and mechanisms of action. Lancet Psychiatry. 2021;8:824–35.
16. Otte C, Gold SM, Penninx BW, Pariante CM, Etkin A, Fava M, et al. Major depressive disorder. Nat Rev Dis Primers. 2016;2:16065.
17. Szuhany KL, Simon NM. Anxiety disorders: a review. JAMA. 2022;328:2431–45.
18. Dunham KE, Venton BJ. SSRI antidepressants differentially modulate serotonin reuptake and release in Drosophila. J Neurochem. 2022;162:404–16.
19. Wood KM, Hashemi P. Fast-scan cyclic voltammetry analysis of dynamic serotonin reponses to acute escitalopram. ACS Chem Neurosci. 2013;4:715–20.
20. Hjorth S. Serotonin 5-HT1A autoreceptor blockade potentiates the ability of the 5-HT reuptake inhibitor citalopram to increase nerve terminal output of 5-HT in vivo: a microdialysis study. J Neurochem. 1993;60:776–9.
21. Dankoski EC, Carroll S, Wightman RM. Acute selective serotonin reuptake inhibitors regulate the dorsal raphe nucleus causing amplification of terminal serotonin release. J Neurochem. 2016;136:1131–41.
22. Doya K, Miyazaki KW, Miyazaki K. Serotonergic modulation of cognitive computations. Curr Opin Behav Sci. 2021;38:116–23.
23. Jackson BP, Dietz SM, Wightman RM. Fast-scan cyclic voltammetry of 5-hydroxytryptamine. Anal Chem. 1995;67:1115–20.
24. Dunham KE, Venton BJ. Improving serotonin fast-scan cyclic voltammetry detection: new waveforms to reduce electrode fouling. Analyst. 2020;145:7437–46.
25. Wan J, Peng W, Li X, Qian T, Song K, Zeng J, et al. A genetically encoded sensor for measuring serotonin dynamics. Nat Neurosci. 2021;24:746–52.
26. Unger EK, Keller JP, Altermatt M, Liang R, Matsui A, Dong C, et al. Directed evolution of a selective and sensitive serotonin sensor via machine learning. Cell. 2020;183:1986–2002.e26.
27. Jing M, Zhang P, Wang G, Feng J, Mesik L, Zeng J, et al. A genetically encoded fluorescent acetylcholine indicator for in vitro and in vivo studies. Nat Biotechnol. 2018;36:726–37.
28. Borden PM, Zhang P, Shivange AV, Marvin JS, Cichon J, Dan C et al. A fast genetically encoded fluorescent sensor for faithful in vivo acetylcholine detection in mice, fish, worms and flies. bioRxiv. 2020; https://www.biorxiv.org/content/10.1101/2020.02.07.939504v1.
29. Bonhaus DW, Weinhardt KK, Taylor M, DeSouza A, McNeeley PM, Szczepanski K, et al. RS-102221: a novel high affinity and selective, 5-HT2C receptor antagonist. Neuropharmacology. 1997;36:621–9.
30. Paquelet GE, Carrion K, Lacefield CO, Zhou P, Hen R, Miller BR. Single-cell activity and network properties of dorsal raphe nucleus serotonin neurons during emotionally salient behaviors. Neuron. 2022;110:2664–2679.e8.
31. Zheng WS, Zhang Y, Zhu RE, Zhang P, Gupta S, Huang L et al. GESIAP: a versatile genetically encoded sensor-based image analysis program. bioRxiv. 2022; https://www.biorxiv.org/content/10.1101/2022.10.05.511006v1.

32. Owens MJ, Knight DL, Nemeroff CB. Second-generation SSRIs: human monoamine transporter binding profile of escitalopram and R-fluoxetine. Biol Psychiatry. 2001;50:345–50.
33. Zhu JJ. Activity level-dependent synapse-specific AMPA receptor trafficking regulates transmission kinetics. J Neurosci. 2009;29:6320–35.
34. Zhu PK, Zheng WS, Zhang P, Jing M, Borden PM, Ali F, et al. Nanoscopic visualization of restricted non-volume cholinergic and monoaminergic transmission with genetically encoded sensors. Nano Lett. 2020;20:4073–83.
35. Zhu RE, Diao X, Liu X, Ru Q, Wu Z, Zhang Z et al. GESIAP3.0: sensor-based image analysis program for transmission visualization in vivo. bioRxiv. 2024; https://www.biorxiv.org/content/10.1101/2024.10.28.620522v1.
36. Fatt P, Katz B. Spontaneous subthreshold activity at motor nerve endings. J Physiol. 1952;117:109–28.
37. Özçete ÖD, Banerjee A, Kaeser PS. Mechanisms of neuromodulatory volume transmission. Mol Psychiatry. 2024;29:3680–93.
38. Miner LH, Schroeter S, Blakely RD, Sesack SR. Ultrastructural localization of the serotonin transporter in superficial and deep layers of the rat prelimbic prefrontal cortex and its spatial relationship to dopamine terminals. J Comp Neurol. 2000;427:220–34.
39. Pickel VM, Chan J. Ultrastructural localization of the serotonin transporter in limbic and motor compartments of the nucleus accumbens. J Neurosci. 1999;19:7356–66.
40. Zhou FC, Tao-Cheng JH, Segu L, Patel T, Wang Y. Serotonin transporters are located on the axons beyond the synaptic junctions: anatomical and functional evidence. Brain Res. 1998;805:241–54.
41. Moncrieff J, Cooper RE, Stockmann T, Amendola S, Hengartner MP, Horowitz MA. The serotonin theory of depression: a systematic umbrella review of the evidence. Mol Psychiatry. 2023;28:3243–56.
42. Kayser C, Melkes B, Derieux C, Bock A. Spatiotemporal GPCR signaling illuminated by genetically encoded fluorescent biosensors. Curr Opin Pharmacol. 2023;71:102384.
43. Yasuda R, Hayashi Y, Hell JW. CaMKII: a central molecular organizer of synaptic plasticity, learning and memory. Nat Rev Neurosci. 2022;23:666–82.
44. Barbour B, Hausser M. Intersynaptic diffusion of neurotransmitter. Trends Neurosci. 1997;20:377–84.
45. Sarter M, Parikh V, Howe WM. Phasic acetylcholine release and the volume transmission hypothesis: time to move on. Nat Rev Neurosci. 2009;10:383–90.
46. Bunin MA, Wightman RM. Quantitative evaluation of 5-hydroxytryptamine (serotonin) neuronal release and uptake: an investigation of extrasynaptic transmission. J Neurosci. 1998;18:4854–60.
47. Hashemi P, Dankoski EC, Lama R, Wood KM, Takmakov P, Wightman RM. Brain dopamine and serotonin differ in regulation and its consequences. Proc Natl Acad Sci USA. 2012;109:11510–5.
48. Ruat M, Traiffort E, Leurs R, Tardivel-Lacombe J, Diaz J, Arrang JM, et al. Molecular cloning, characterization, and localization of a high-affinity serotonin receptor (5-HT7) activating cAMP formation. Proc Natl Acad Sci USA. 1993;90:8547–51.
49. Yamamoto T, Ochalski A, Hertzberg EL, Nagy JI. On the organization of astrocytic gap junctions in rat brain as suggested by LM and EM immunohistochemistry of connexin43 expression. J Comp Neurol. 1990;302:853–83.
50. Chazal G, Ralston HJ 3rd. Serotonin-containing structures in the nucleus raphe dorsalis of the cat: an ultrastructural analysis of dendrites, presynaptic dendrites, and axon terminals. J Comp Neurol. 1987;259:317–29.
51. Herve D, Pickel VM, Joh TH, Beaudet A. Serotonin axon terminals in the ventral tegmental area of the rat - fine-structure and synaptic Input to dopaminergic neurons. Brain Res. 1987;435:71–83.
52. Papadopoulos GC, Parnavelas JG, Buijs R. Monoaminergic fibers form conventional synapses in the cerebral cortex. Neurosci Lett. 1987;76:275–9.
53. Fitzgerald LW, Conklin DS, Krause CM, Marshall AP, Patterson JP, Tran DP, et al. High-affinity agonist binding correlates with efficacy (intrinsic activity) at the human serotonin 5-HT2A and 5-HT2C receptors: evidence favoring the ternary complex and two-state models of agonist action. J Neurochem. 1999;72:2127–34.
54. Kumar JS, Milak MS, Majo VJ, Prabhakaran J, Mali P, Savenkova L, et al. Comparison of high and low affinity serotonin 1A receptors by PET in vivo in non-human primates. J Pharmacol Sci. 2012;120:254–7.
55. Wu Z, Lin D, Li Y. Pushing the frontiers: tools for monitoring neurotransmitters and neuromodulators. Nat Rev Neurosci. 2022;23:257–74.
56. Marcott PF, Mamaligas AA, Ford CP. Phasic dopamine release drives rapid activation of striatal D2-receptors. Neuron. 2014;84:164–76.
57. Greengard P. The neurobiology of slow synaptic transmission. Science. 2001;294:1024–30.
58. Sudhof TC. The cell biology of synapse formation. J Cell Biol. 2021;220:e202103052.
59. Wu LG, Hamid E, Shin W, Chiang HC. Exocytosis and endocytosis: modes, functions, and coupling mechanisms. Annu Rev Physiol. 2014;76:301–31.

60. von Gersdorff H, Borst JGG. Short-term plasticity at the calyx of held. Nat Rev Neurosci. 2002;3:53–64.

61. Pulido C, Marty A. Quantal fluctuations in central mammalian synapses: functional role of vesicular docking sites. Physiological Rev. 2017;97:1403–30.

62. Edwards FA, Konnerth A, Sakmann B. Quantal analysis of inhibitory synaptic transmission in the dentate gyrus of rat hippocampal slices: a patch-clamp study. J Physiol. 1990;430:213–49.

63. Stern P, Edwards FA, Sakmann B. Fast and slow components of unitary EPSCs on stellate cells elicited by focal stimulation in slices of rat visual cortex. J Physiol. 1992;449:247–78.

64. Jonas P, Major G, Sakmann B. Quantal components of unitary EPSCs at the mossy fibre synapse on CA3 pyramidal cells of rat hippocampus. J Physiol. 1993;472:615–63.

65. Malinow R, Malenka RC. AMPA receptor trafficking and synaptic plasticity. Annu Rev Neurosci. 2002;25:103–26.

66. Volk L, Chiu SL, Sharma K, Huganir RL. Glutamate synapses in human cognitive disorders. Annu Rev Neurosci. 2015;38:127–49.

67. Connor SA, Siddiqui TJ. Synapse organizers as molecular codes for synaptic plasticity. Trends Neurosci. 2023;46:971–85.

68. Lin L, Gupta S, Zheng WS, Si K, Zhu JJ. Genetically encoded sensors enable micro- and nano-scopic decoding of transmissions in healthy and diseased brains. Mol Psychiatry. 2021;26:443–55.

69. Chen J, Cho KE, Skwarzynska D, Clancy S, Conley NJ, Clinton SM, et al. The property-based practical applications and solutions of genetically encoded acetylcholine and monoamine sensors. J Neurosci. 2021;41:2318–28.

70. Sun N, Qin YJ, Xu C, Xia T, Du ZW, Zheng LP, et al. Design of fast-onset antidepressant by dissociating SERT from nNOS in the DRN. Science. 2022;378:390–8.

71. Scott MM, Wylie CJ, Lerch JK, Murphy R, Lobur K, Herlitze S, et al. A genetic approach to access serotonin neurons for in vivo and in vitro studies. Proc Natl Acad Sci USA. 2005;102:16472–7.

72. Zhang L, Zhang P, Wang G, Zhang H, Zhang Y, Yu Y, et al. Ras and Rap signal bidirectional synaptic plasticity via distinct subcellular microdomains. Neuron. 2018;98:783–800.

73. Wang G, Zhang P, Mendu SK, Wang Y, Zhang Y, Kang X, et al. Revaluation of magnetic properties of Magneto. Nat Neurosci. 2020;23:1047–50.

74. Huang L, Chen Y, Jin S, Lin L, Duan S, Si K, et al. Organizational principles of amygdalar input-output neuronal circuits. Mol Psychiatry. 2021;26:7118–29.

75. Wang G, Wyskiel DR, Yang W, Wang Y, Milbern LC, Lalanne T, et al. An optogenetics- and imaging-assisted simultaneous multiple patch-clamp recordings system for decoding complex neural circuits. Nat Protoc. 2015;10:397–412.

76. Weigert M, Schmidt U, Boothe T, Muller A, Dibrov A, Jain A, et al. Content-aware image restoration: pushing the limits of fluorescence microscopy. Nat Methods. 2018;15:1090–7.

77. Arigovindan M, Fung JC, Elnatan D, Mennella V, Chan YH, Pollard M, et al. High-resolution restoration of 3D structures from widefield images with extreme low signal-to-noise-ratio. Proc Natl Acad Sci USA. 2013;110:17344–9.

78. Koho S, Tortarolo G, Castello M, Deguchi T, Diaspro A, Vicidomini G. Fourier ring correlation simplifies image restoration in fluorescence microscopy. Nat Commun. 2019;10:3103.

79. Wernersson E, Gelali E, Girelli G, Wang S, Castillo D, Mattsson Langseth C, et al. Deconwolf enables high-performance deconvolution of widefield fluorescence microscopy images. Nat Methods. 2024;21:1–12.

80. Hashemi P, Walsh PL, Guillot TS, Gras-Najjar J, Takmakov P, Crews FT, et al. Chronically implanted, Nafion-coated Ag/AgCl reference electrodes for neurochemical applications. ACS Chem Neurosci. 2011;2:658–66.

81. Stucky C, Johnson MA. Improved serotonin measurement with fast-scan cyclic voltammetry: mitigating fouling by SSRIs. J Electrochem Soc. 2022;169:045501.

82. Zhu JJ. Architectural organization of ~1500-neuron modular minicolumnar disinhibitory circuits in healthy and Alzheimer's cortices. Cell Rep. 2023;42:112904.

83. Privman E, Venton BJ. Comparison of dopamine kinetics in the larval Drosophila ventral nerve cord and protocerebrum with improved optogenetic stimulation. J Neurochem. 2015;135:695–704.

AUTHOR CONTRIBUTIONS
BJV and JJZ conceived the concept of multiplexed sensor-based imaging and FSCV method, and JJZ also conceived the concept of nanoscopic analysis of serotonergic transmission modes; JJZ led the project at the University of Virginia before July 1, 2024, and continued leading it at Wenzhou Medical University after leaving UVA; JJZ designed the experiments with input from YZ; YZ and YC performed experiments revealing the regulation of serotonergic transmission modes, and PZ and MS performed initial experiments establishing and validating the multiplexed imaging and FSCV method; YZ and PZ analyzed image data, and MS, YC, and BJV analyzed FSCV data; JJZ wrote the manuscript with input from all other coauthors.

COMPETING INTERESTS
The authors declare no competing interests.

ADDITIONAL INFORMATION
Supplementary information The online version contains supplementary material available at https://doi.org/10.1038/s41380-025-02930-4.

Correspondence and requests for materials should be addressed to J. Julius Zhu.

Reprints and permission information is available at http://www.nature.com/reprints

Publisher's note Springer Nature remains neutral with regard to jurisdictional claims in published maps and institutional affiliations.